

Bulk-Fermi-Arc Transition Induced Large Photogalvanic Effect in Weyl Semimetals

Jin Cao,^{1,2,*} Maoyuan Wang,^{1,2,*} Zhi-Ming Yu,^{1,2,†} and Yugui Yao^{1,2,‡}

¹Centre for Quantum Physics, Key Laboratory of Advanced Optoelectronic Quantum Architecture and Measurement (MOE), School of Physics, Beijing Institute of Technology, Beijing, 100081, China

²Beijing Key Lab of Nanophotonics & Ultrafine Optoelectronic Systems, School of Physics, Beijing Institute of Technology, Beijing, 100081, China

The surface Fermi arc, as a hallmark of Weyl semimetals (WSMs), has been well known in current research, but it remains a challenge to unveil novel phenomena associated with the Fermi arc. Here, we predict a heretofore unrecognized process in WSMs, namely, the photoinduced transition between the bulk states and the Fermi arc. We find this process is significant and can lead to a large effective three-dimensional shift current on the boundaries with the Fermi arc in wide terahertz range. Moreover, due to the low symmetry of the boundaries, the surface photogalvanic effect predicted here can appear in a large class of WSMs that do not have bulk shift current. Hence, our work not only unveils a hidden photogalvanic effect in WSMs but also suggests that all the WSMs are promising material candidates for developing efficient terahertz photodetectors.

Introduction. The photogalvanic effect refers to the generation of dc electric current in a material illuminated by light [1]. It has been attracting intensive interest in condensed matter physics, due to the promising application on photodetectors and solar cells beyond pn junction structure [2–10]. In addition to technological application, the photogalvanic effect also provides a basic mechanism to probe various geometric quantities of systems, such as the Berry curvature, quantum metric and Christoffel symbols [11–19].

Generally, the dominant dc response of materials under a monochromatic light characterized by $\mathbf{A}(t) = \mathbf{A}(\omega) e^{-i\omega t} + c.c.$ is quadratic, and the shift current, a representative photogalvanic effect, can be expressed as [11]

$$j^a = \sigma_{bc}^a(\omega) E^b(\omega) E^c(-\omega), \quad (1)$$

with σ_{bc}^a the third-rank shift conductivity tensor and $\mathbf{E}(\omega) = i\omega \mathbf{A}(\omega)$. Here, we have adopted the Einstein summation convention and the roman letters a, b, \dots denote Cartesian indexes. Clearly, the tensor σ_{bc}^a is constrained by the (magnetic) point group of the systems. For example, when the system has spatial inversion symmetry \mathcal{P} , σ_{bc}^a should vanish, as both \mathbf{j} and \mathbf{E} change sign under \mathcal{P} . Hence, the studies of shift current effect generally focus on noncentrosymmetric materials [20, 21].

Many efforts have been devoted to searching material candidates with large shift current effect. For example, A. M. Cook *et al.* [22] predicted that the shift current in the semiconductors with semi-Dirac type of Hamiltonian is large and may compete with conventional solar cells based on pn junction. T. Rangel *et al.* [23] confirmed it by performing first-principles calculations on single-layer monochalcogenides with such low-energy Hamiltonian and found the effective three-dimensional shift con-

ductivity in these materials is larger than that in many other polar systems.

Currently, the exploration is extended to topological WSMs [24–39]. For WSMs, the conduction band and the valence band form Weyl points in the bulk, around which all the geometric quantities become divergent, and the topological surface Fermi arc state appears on the boundaries [40, 41]. Since the shift current is closely related to the shift vector and the Christoffel symbols [11, 18], one can expect that the shift current in WSM may be significant. Moreover, the gapless feature makes WSMs an ideal choice for designing terahertz photodetectors [21, 27]. However, as aforementioned the shift current is constrained by the symmetries of system. Besides \mathcal{P} symmetry, an emergent SO(3) rotational symmetry, which typically exists for the Weyl points at high-symmetry points under certain space group symmetries [42, 43], would also cause the shift current to vanish [18]. Thus, a large class of WSMs are forbidden by symmetries to have net bulk shift current. There also exist few works that studied the photogalvanic effect on the boundary of the topological materials, focusing on the photocurrent solely induced by the topological surface states [44–49]. But the shift current effect there generally are not significant.

In this work, we show that large surface shift current can be generated by a unique and heretofore unrecognized process in WSMs, namely, the transition between bulk states and the surface Fermi arc. This process is termed as bulk-Fermi-arc transition. A key observation is that the surface Fermi arc is always attached to the bulk Weyl cones at any energy [40], and there exists considerable overlap between the bulk states and the part of the Fermi arc attached to the bulk [50], as illustrated in Fig. 1(a). Hence, considerable bulk-Fermi-arc transition should widely occur in WSMs.

We first establish a local second-order response formula, and then use it to study the surface shift current of a WSM with \mathcal{P} symmetry and only one pair of Weyl

* These authors contributed equally to this work.

† zhiming-yu@bit.edu.cn

‡ ygyao@bit.edu.cn

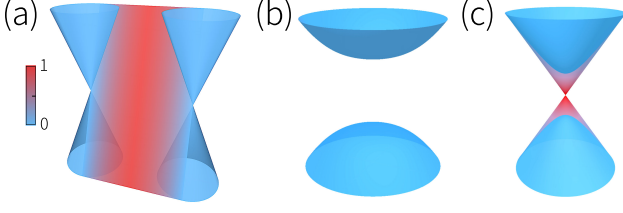


FIG. 1. Three typical band structures. (a) Weyl semimetal with surface Fermi arc. (b) Trivial insulator and (c) topological insulator with topological surface state. The blue surfaces denote bulk bands. The surface states in (a) and (c) are attached to the bulk bands. The color map in surface states indicates the weight of projection onto surface. Considerable transition between bulk and surface states would widely appear in (a), while can not happen for (b) and happen in (c) for certain doping.

points. In this WSM model, both the bulk shift current and the surface shift current solely from the surface Fermi arc are zero. Surprisingly, we find that significant surface shift current effect can occur and only occur on the boundaries with Fermi arc, indicating that this considerable large shift current is induced by the bulk-Fermi-arc transition. Particularly, the absolute value of the effective three-dimensional shift current induced by the bulk-Fermi-arc transition can exceed $100 \mu\text{A}/\text{V}^2$ in a wide terahertz range, due to the gapless spectrum between the bulk and the Fermi arc [see Fig. 1(a)]. Such large shift current is comparable with that in the single-layer monochalcogenides [23] and the bulk shift current in the previously studied topological semimetals [35]. Moreover, due to the low symmetry on the boundary, the surface shift current effect predicted here generally would appear in all kinds of the WSMs, including a large class of WSMs that do not have net shift current in bulk. This greatly relaxes the applied restrictions of WSM in terahertz photodetectors.

Local photocurrent response. We first establish a general formula to describe the local photocurrent response to study spatially resolved shift current effect. The space dependent current operator generally can be written as [51]

$$J_a(\mathbf{r}) = -\frac{e}{2V} \sum_{\mu\nu, \mathbf{r}'} v_{\mu\mathbf{r}, \nu\mathbf{r}'}^a d_{\mu\mathbf{r}}^\dagger d_{\nu\mathbf{r}'} + h.c., \quad (2)$$

which counts all of the currents flowing from \mathbf{r}' to \mathbf{r} . Here, V is the volume of system, e denotes the charge carried by an electron, $d_{\mu\mathbf{r}}^\dagger$ ($d_{\mu\mathbf{r}}$) creates (annihilates) a localized Wannier state $w_{\mu\mathbf{r}}$ at \mathbf{r} with basis orbit μ , and $v_{\mu\mathbf{r}, \nu\mathbf{r}'}^a = \frac{1}{2m} \langle w_{\mu\mathbf{r}} | -i\partial_a | w_{\nu\mathbf{r}'} \rangle$ with m the mass of the electrons. The eigenstates are constructed from the Wannier states by $c_n^\dagger = \sum_{\mu\mathbf{r}} U_{\mu\mathbf{r}, n} d_{\mu\mathbf{r}}^\dagger$ with n a combined index denoting energy band and momentum (if the sys-

tem has translation symmetry), it then follows

$$J_a(\mathbf{r}) = -\frac{e}{V} \sum_{mn} v_{mn}^a(\mathbf{r}) c_m^\dagger c_n, \quad (3)$$

where $v_{mn}^a(\mathbf{r})$ is the local velocity operator matrix, defined as

$$v_{mn}^a(\mathbf{r}) \equiv \frac{1}{2} \sum_{\mu\nu, \mathbf{r}'} U_{m, \mu\mathbf{r}}^\dagger v_{\mu\mathbf{r}, \nu\mathbf{r}'}^a U_{\nu\mathbf{r}', n} + h.c.. \quad (4)$$

Consider a slab model with y -direction being confined and assuming the model is uniformly illuminated by monochromatic light of frequency ω . The applied light (electric) field can be introduced into the Hamiltonian by velocity-gauge approach, $H' = -\int d\mathbf{r} \mathbf{J}(\mathbf{r}) \cdot \mathbf{A}(\mathbf{r}, t)$. According to the standard perturbation procedure, the local shift conductivity can be established as (see supplemental materials (SM) [52])

$$\sigma_{bc}^a(\omega; y) = -\frac{\pi e^3}{2L\omega^2} \text{Im} \int \frac{dk_x dk_z}{(2\pi)^2} \sum_{y', y''} \sum_{lmn; \pm\omega} \frac{f_{nl}}{\varepsilon_{lm}} \times v_{lm, y}^a (v_{mn, y'}^b v_{nl, y''}^c + v_{mn, y''}^c v_{nl, y'}^b) \delta(\varepsilon_{ln} - \hbar\omega), \quad (5)$$

where L is the thickness of the slab, $f_{nl} = f_n - f_l$ and $\varepsilon_{lm} = \varepsilon_l - \varepsilon_m$ are the occupation and the energy differences between the two states involved in the optical transition, f_n is the Fermi-Dirac distribution. Since Eq. (5) has the form of Fermi golden rule, the shift current effect is a interband effect.

For top surface, the effective three-dimensional shift conductivity may be defined as

$$\Sigma_{bc}^a(\omega) = \frac{1}{l} \int_{L/2-l}^{L/2} dy \sigma_{bc}^a(\omega; y), \quad (6)$$

where $l \ll L$ is the distance measured from the top surface at $L/2$. The conductivity for bottom surface can be similarly defined. When the system has \mathcal{P} symmetry, the surface shift conductivity for the top and bottom surfaces would take opposite values. While the value of $\Sigma_{bc}^a(\omega)$ has a dependence on l , the qualitative behaviors of $\Sigma_{bc}^a(\omega)$ would be robust against the choice of l .

Weyl model. Since our goal is to demonstrate the existence of the surface photocurrent induced by bulk-Fermi-arc transition, we take a simplest WSM model with only two conventional Weyl points without energy tilt at Fermi level. The essential physics learned here applies to general WSMs and other topological semimetals with surface Fermi arc. We also assume the system has \mathcal{P} symmetry to exclude the bulk photocurrent. This indicates the WSM model has to break time-reversal symmetry (\mathcal{T}), while a combined operator \mathcal{OT} with \mathcal{O} a certain spatial operator may be persevered. Since there exists (at most) only one surface Fermi arc on each boundary of system, the surface shift current solely from the Fermi arc would be zero.

Consider a tight-binding model defined on a cubic lattice

$$\mathcal{H}_W(\mathbf{k}) = [\Delta + t_1(\cos k_x + \cos k_y) + t_2 \cos k_z] \sigma_z + t_3(\sin k_x \sigma_x + \sin k_y \sigma_y), \quad (7)$$

where σ_i 's are the Pauli matrixes, $t_1 = t_2 = 1.0 \text{ eV}$, $t_3 = 0.25 \text{ eV}$ and $\Delta = \Delta_0 - 2t_1 - t_2$ with $\Delta_0 = 0.5 \text{ eV}$. This lattice model (7) has only two Weyl points on the k_z axis at $k_z^\pm = \pm \arccos(2\Delta_0/t_1)$. These two Weyl points are conventional linear Weyl points with Chern number $C = \pm 1$. In the bulk, the symmetries of the lattice model are generated by \mathcal{P} symmetry, a mirror \mathcal{M}_z , a fourfold rotation \mathcal{C}_{4z} and a combined operator $\mathcal{C}_{2y}\mathcal{T}$, which respectively can be represented as $\mathcal{P} = \sigma_z$, $\mathcal{M}_z = i\sigma_0$, $\mathcal{C}_{4z} = \frac{\sigma_0 + i\sigma_3}{\sqrt{2}}$ and $\mathcal{C}_{2y}\mathcal{T} = \mathcal{K}$.

The calculated band structure from Eq. (7) is plotted in Fig. 2(a), together with the surface Fermi arc on the (010) surface. One observes that the two Weyl points locate at $k_z^\pm \hat{\mathbf{z}}$ points respectively. Moreover, the bands of the two Weyl points are connected at a higher (lower) energy to form a saddle surface around k_x axis. At low energy, the surface Fermi arc is attached to the Weyl cones, as discussed above [see Fig. 1(a)]. Besides, the Fermi arc would also merge into the bulk saddle surface at higher (lower) energy. Thus, there generally exist two different photoinduced bulk-Fermi-arc transitions in WSMs, namely, one is the transition from the Weyl points to the Fermi arc and other is from the saddle surface to the Fermi arc.

Surface shift current. We then study the shift current on the (010) surface of the lattice model (7) under an uniform irradiation of a linearly polarized light. The nonzero components of the surface shift conductivity tensors are determined by the magnetic point group of the (010) surface, which are generated by \mathcal{M}_z and $\mathcal{C}_{2y}\mathcal{T}$. Then the shift conductivity tensors, that are odd under the mirror \mathcal{M}_z , namely, $\sigma_{xz}^x, \sigma_{yz}^x, \sigma_{xz}^z, \sigma_{yz}^z, \sigma_{zz}^x, \sigma_{zz}^z, \sigma_{xy}^x, \sigma_{xy}^z$ and $\sigma_{yz}^x, \sigma_{yz}^z, \sigma_{xz}^x, \sigma_{xz}^z, \sigma_{zz}^x, \sigma_{zz}^z, \sigma_{xy}^x, \sigma_{xy}^z$ are excluded by $\mathcal{C}_{2y}\mathcal{T}$. Thus, there are only four symmetry allowed tensors and two of them are independent, which are $\sigma_{xy}^x = \sigma_{yx}^x$ and $\sigma_{zy}^z = \sigma_{yz}^z$.

Using the established formula (5), we calculate the local shift conductivities $\sigma_{xy}^x(\omega; y)$ and $\sigma_{zy}^z(\omega; y)$ for a (010) slab with a thickness of $L = 101 L_s$. Here, L_s is the thickness of a unit cell. The obtained results of the local shift conductivities regarding with ω are shown in Fig. 2(b) and 2(c). One finds that both $\sigma_{xy}^x(\omega; y)$ and $\sigma_{zy}^z(\omega; y)$ are finite for a generic layer of the slab, as a generic layer has the same symmetry conditions as the (010) surface. Remarkably, the two conductivities not only are sizable but also can feature strong surface enhancement behavior for certain frequencies, leading to significant photogalvanic effect on the (010) surface. For clarity, we calculate the top surface shift conductivities $\Sigma_{xy}^x(\omega)$ and $\Sigma_{zy}^z(\omega)$ with $l = 4 L_s$, and find they can

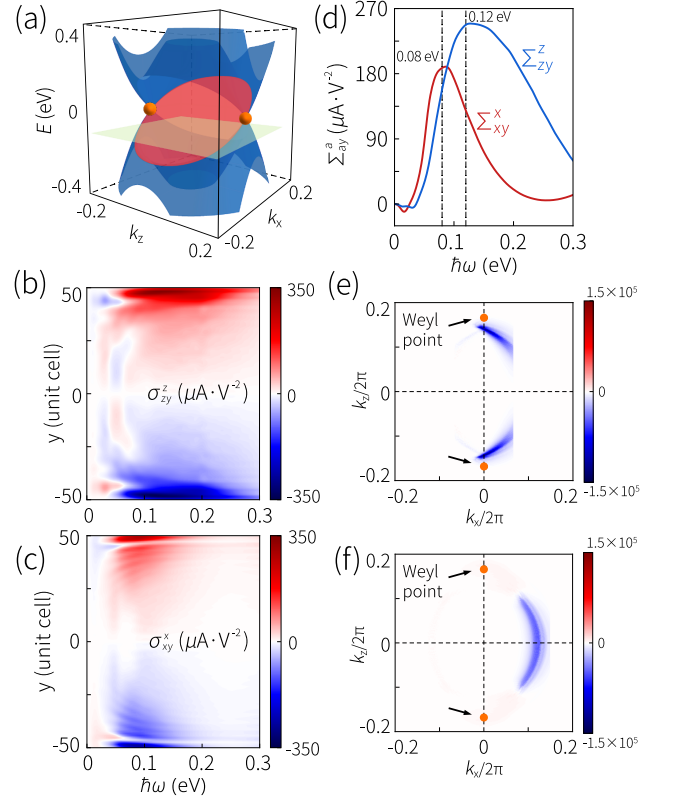


FIG. 2. (a) Band structure of the model (7) at $k_y = 0$ plane (blue surfaces), together with the surface Fermi arc states at (010) surface (red surface). Green surface denotes the Fermi level. (b,c) show the local shift conductivity $\sigma_{zy}^z(\omega; y)$ and $\sigma_{xy}^x(\omega; y)$ for the (010) slab, where significant surface enhancement can be observed. We set $E_F = -0.1 \text{ eV}$ in (b), $E_F = -0.2 \text{ eV}$ in (c). (d) shows the two surface shift conductivities which are obtained from (b) and (c) with $l = 4 L_s$. (e-f) The distribution of $\sigma_{zy}^z(\omega; y = L/2)$ and $\sigma_{xy}^x(\omega; y = L/2)$ in the (010) surface BZ. We set $E_F = -0.1 \text{ eV}$ and $\hbar\omega = 0.12 \text{ eV}$ in (e), and $E_F = -0.2 \text{ eV}$ and $\hbar\omega = 0.08 \text{ eV}$ in (f).

be larger than $100 \mu\text{A}/\text{V}^2$ in a wide frequency range, as shown in Fig. 2(d). Such large surface shift conductivities to our best knowledge has never been reported before. Moreover, the peak of both $\Sigma_{xy}^x(\omega)$ and $\Sigma_{zy}^z(\omega)$ appear around terahertz range ($\hbar\omega \sim 100 \text{ meV}$), indicating that the surface photogalvanic effect predicted here can be used to design efficient infrared and terahertz photodetectors.

To further study the significant surface photogalvanic effect, we calculate the distribution of the local conductivities $\sigma_{zy}^z(\omega; y = L/2)$ and $\sigma_{xy}^x(\omega; y = L/2)$ that exhibit strong surface enhancement behavior in the 2D Brillouin zone (BZ) of the (010) slab. The results are shown in Fig. 2(e) and 2(f). Interestingly, the distribution for both conductivities concentrates around the Fermi arc, indicating the enhanced surface shift current is closely related to the Bulk-Fermi-arc transition. However, the large contribution for σ_{zy}^z comes from the tran-

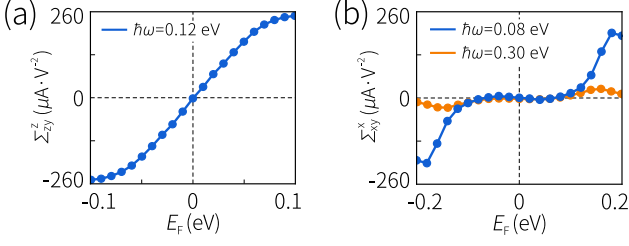


FIG. 3. The (010) surface shift conductivities (a) Σ_{zy}^z and (b) Σ_{xy}^x of the Weyl model (7) versus the Fermi level.

sition between the two Weyl points and the Fermi arc [see Fig. 2(e)], while for σ_{xy}^x is from the transition between the saddle surface and the arc [see Fig. 2(f)]. This difference will lead to completely different low-energy behavior of the two surface conductivities.

When the Fermi level exactly locates at Weyl points $E_F = 0$, the model (7) has an emergent particle-hole symmetry $\mathcal{C} = \sigma_x \mathcal{K}$ with $\mathcal{C} \mathcal{H}_W(\mathbf{k}) \mathcal{C}^{-1} = -\mathcal{H}_W(-\mathbf{k})$, in such case all the shift conductivities would vanish, as the particle-hole symmetry reverses the direction of the photocurrent [18]. Deviating from the neutral filling point, the absolute value of $\Sigma_{zy}^z(\omega)$ will increase rapidly [see Fig. 3(a)]. In contrast, $\Sigma_{xy}^x(\omega)$ will still be almost vanishing at low energy $|E_F| < 0.1$ eV for any frequency [see Fig. 3(b)]. The vanishing $\Sigma_{xy}^x(\omega)$ is because that at low energy, the Fermi arc near k_x axis is mainly localized on the surface and has vanishing overlap with the bulk state [see Fig. 2(a)]. $\Sigma_{xy}^x(\omega)$ becomes significant only when the Fermi level approaches the bulk saddle surface and the frequency $\hbar\omega$ is at terahertz range, as shown in Fig. 3(b). This again demonstrates that only the part of the Fermi arc connected to the bulk states can have a considerable overlap with the bulk states, and then the bulk-Fermi-arc transition is promoted.

For comparison, we also calculate the local shift conductivity for the (001) slab of the WSM model (7) under same parameters. For (001) surface, only one shift current conductivity $\sigma_{xz}^x(\omega; z)$ is independent (see SM [52]). Unlike the (010) surface, the (001) surface does not have a Fermi arc because the two Weyl points are projected

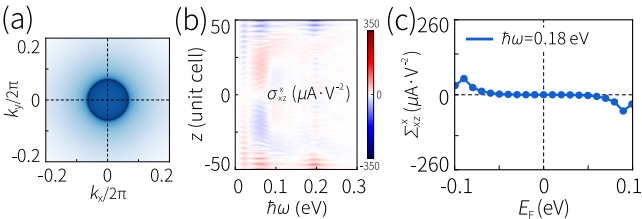


FIG. 4. (a) Surface spectra on (001) surface of the lattice model (7). (b) The local shift conductivity $\sigma_{xz}^x(\omega; z)$ for the (001) slab. In (a) and (b), we set $E_F = -0.1$ eV. (c) The (001) surface shift conductivity versus the Fermi level.

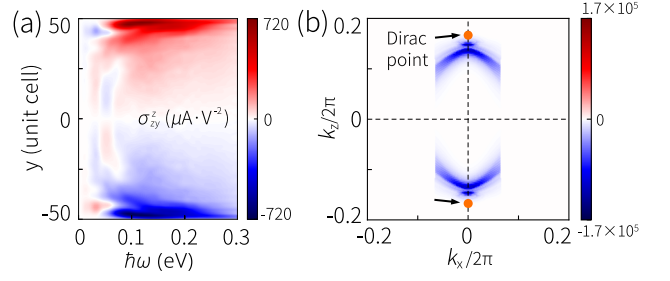


FIG. 5. (a) The local shift conductivity $\sigma_{zy}^z(\omega; y)$ for the (010) slab of the Dirac model (8). (b) shows the distribution of $\sigma_{zy}^z(\omega; y = L/2)$ in the (010) surface BZ. We set $c_1 = c_2 = 0.1$ eV, $E_F = -0.1$ eV in (a) and (b), and set $\hbar\omega = 0.12$ eV in (b).

to the same point in the BZ of the (001) surface [see Fig. 4(a)]. We find that for different $\hbar\omega$ and E_F , the $\sigma_{xz}^x(\omega; z)$ does not feature significant surface enhancement behavior, and the obtained surface shift conductivity is much smaller than that in (010) surface, as shown in Fig. 4(b) and 4(c). These results unambiguously demonstrate the significant surface photogalvanic effect in WSMs is induced by the bulk-Fermi-arc transition.

Discussions. In this work, we use a WSM model to demonstrate the existence of the large surface photovoltaic effect induced by the bulk-Fermi-arc transition. Actually, this effect would generally exist in all the topological semimetals with surface Fermi arc. As an example, we consider a Dirac semimetals with \mathcal{P} and \mathcal{T} ,

$$\mathcal{H}_D(\mathbf{k}) = \begin{bmatrix} \mathcal{H}_W(\mathbf{k}) & h_{12} \\ h_{12}^\dagger & \mathcal{H}_W^*(-\mathbf{k}) \end{bmatrix}, \quad (8)$$

with

$$h_{12} = -2c_1 \sin k_z (\cos k_x - \cos k_y) \sigma_x + c_2 \sin k_x \sin k_y \sin k_z \sigma_y. \quad (9)$$

This model gives a pair of Dirac points at k_z axis and two Fermi arcs on the (010) surface, which respectively occupy different parts of the (010) surface BZ (see SM [52]). Thus, for the model (8), the shift current solely from both the bulk and the surface Fermi arcs vanishes. The calculated results of $\sigma_{zy}^z(\omega; y)$ for the (010) slab of the Dirac model (8) are given in Fig. 5. Similar to the cases in WSM (7), $\sigma_{zy}^z(\omega; y)$ here also exhibits strong surface enhancement and the distribution for $\sigma_{zy}^z(\omega; y = L/2)$ mainly concentrates around the two Fermi arcs, showing the surface photocurrent in model (8) also is induced by the bulk-Fermi-arc transition.

The experimental detection of the surface shift current effect has been well developed [48, 53], and many materials are experimentally confirmed as topological (Weyl) semimetals with surface Fermi arc [54–61]. Hence, the novel effect predicted here should be readily probed in experiments.

The authors thank S. A. Yang, Rui-Chun Xiao and J. Xun for helpful discussions. This work is supported by the National Key R&D Program of China (Grants No. 2020YFA0308800), the NSF of China (Grants No. 11734003, No. 12061131002 and No. 12004035), the Strategic Priority Research Program of the Chinese Academy of Sciences (Grant No. XDB30000000), and the Beijing Institute of Technology Research Fund Program for Young Scholars.

-
- [1] R. W. Boyd, *Nonlinear Optics* (Academic press, 1992).
 - [2] S. M. Young and A. M. Rappe, First principles calculation of the shift current photovoltaic effect in ferroelectrics, *Phys. Rev. Lett.* **109**, 116601 (2012).
 - [3] S. M. Young, F. Zheng, and A. M. Rappe, First-principles calculation of the bulk photovoltaic effect in bismuth ferrite, *Phys. Rev. Lett.* **109**, 236601 (2012).
 - [4] C. Somma, K. Reimann, C. Flytzanis, T. Elsaesser, and M. Woerner, High-field terahertz bulk photovoltaic effect in lithium niobate, *Phys. Rev. Lett.* **112**, 146602 (2014).
 - [5] M. Nakamura, S. Horiuchi, F. Kagawa, N. Ogawa, T. Kurumaji, Y. Tokura, and M. Kawasaki, Shift current photovoltaic effect in a ferroelectric charge-transfer complex, *Nature Communications* **8**, 281 (2017).
 - [6] C. Wang, X. Liu, L. Kang, B.-L. Gu, Y. Xu, and W. Duan, First-principles calculation of nonlinear optical responses by wannier interpolation, *Phys. Rev. B* **96**, 115147 (2017).
 - [7] A. Ghalgaoui, K. Reimann, M. Woerner, T. Elsaesser, C. Flytzanis, and K. Biermann, Resonant second-order nonlinear terahertz response of gallium arsenide, *Phys. Rev. Lett.* **121**, 266602 (2018).
 - [8] A. M. Burger, R. Agarwal, A. Aprelev, E. Schrubba, A. Gutierrez-Perez, V. M. Fridkin, and J. E. Spanier, Direct observation of shift and ballistic photovoltaic currents, *Science Advances* **5**, 10.1126/sciadv.aau5588 (2019).
 - [9] S. R. Panday, S. Barraza-Lopez, T. Rangel, and B. M. Fregoso, Injection current in ferroelectric group-iv monochalcogenide monolayers, *Phys. Rev. B* **100**, 195305 (2019).
 - [10] H. Wang and X. Qian, Ferrocity-driven nonlinear photocurrent switching in time-reversal invariant ferroic materials, *Science Advances* **5**, 10.1126/sciadv.aav9743 (2019).
 - [11] J. E. Sipe and A. I. Shkrebtii, Second-order optical response in semiconductors, *Phys. Rev. B* **61**, 5337 (2000).
 - [12] T. Morimoto, S. Zhong, J. Orenstein, and J. E. Moore, Semiclassical theory of nonlinear magneto-optical responses with applications to topological dirac/weyl semimetals, *Phys. Rev. B* **94**, 245121 (2016).
 - [13] T. Morimoto and N. Nagaosa, Topological nature of nonlinear optical effects in solids, *Science Advances* **2**, 10.1126/sciadv.1501524 (2016).
 - [14] N. Nagaosa and T. Morimoto, Concept of quantum geometry in optoelectronic processes in solids: Application to solar cells, *Advanced Materials* **29**, 1603345 (2017).
 - [15] B. M. Fregoso, T. Morimoto, and J. E. Moore, Quantitative relationship between polarization differences and the zone-averaged shift photocurrent, *Phys. Rev. B* **96**, 075421 (2017).
 - [16] B. M. Fregoso, R. A. Muniz, and J. E. Sipe, Jerk current: A novel bulk photovoltaic effect, *Phys. Rev. Lett.* **121**, 176604 (2018).
 - [17] D. E. Parker, T. Morimoto, J. Orenstein, and J. E. Moore, Diagrammatic approach to nonlinear optical response with application to weyl semimetals, *Phys. Rev. B* **99**, 045121 (2019).
 - [18] J. Ahn, G.-Y. Guo, and N. Nagaosa, Low-frequency divergence and quantum geometry of the bulk photovoltaic effect in topological semimetals, *Phys. Rev. X* **10**, 041041 (2020).
 - [19] T. Holder, D. Kaplan, and B. Yan, Consequences of time-reversal-symmetry breaking in the light-matter interaction: Berry curvature, quantum metric, and diabatic motion, *Phys. Rev. Research* **2**, 033100 (2020).
 - [20] J. Liu, F. Xia, D. Xiao, F. J. García de Abajo, and D. Sun, Semimetals for high-performance photodetection, *Nature Materials* **19**, 830 (2020).
 - [21] N. Nagaosa, T. Morimoto, and Y. Tokura, Transport, magnetic and optical properties of weyl materials, *Nature Reviews Materials* **5**, 621 (2020).
 - [22] A. M. Cook, B. M. Fregoso, F. de Juan, S. Coh, and J. E. Moore, Design principles for shift current photovoltaics, *Nature Communications* **8**, 14176 (2017).
 - [23] T. Rangel, B. M. Fregoso, B. S. Mendoza, T. Morimoto, J. E. Moore, and J. B. Neaton, Large bulk photovoltaic effect and spontaneous polarization of single-layer monochalcogenides, *Phys. Rev. Lett.* **119**, 067402 (2017).
 - [24] H. Ishizuka, T. Hayata, M. Ueda, and N. Nagaosa, Emergent electromagnetic induction and adiabatic charge pumping in noncentrosymmetric weyl semimetals, *Phys. Rev. Lett.* **117**, 216601 (2016).
 - [25] K. Taguchi, T. Imaeda, M. Sato, and Y. Tanaka, Photovoltaic chiral magnetic effect in weyl semimetals, *Phys. Rev. B* **93**, 201202 (2016).
 - [26] F. de Juan, A. G. Grushin, T. Morimoto, and J. E. Moore, Quantized circular photogalvanic effect in weyl semimetals, *Nature Communications* **8**, 15995 (2017).
 - [27] C.-K. Chan, N. H. Lindner, G. Refael, and P. A. Lee, Photocurrents in weyl semimetals, *Phys. Rev. B* **95**, 041104 (2017).
 - [28] E. J. König, H.-Y. Xie, D. A. Pesin, and A. Levchenko, Photogalvanic effect in weyl semimetals, *Phys. Rev. B* **96**, 075123 (2017).
 - [29] Q. Ma, S.-Y. Xu, C.-K. Chan, C.-L. Zhang, G. Chang, Y. Lin, W. Xie, T. Palacios, H. Lin, S. Jia, P. A. Lee, P. Jarillo-Herrero, and N. Gedik, Direct optical detection of weyl fermion chirality in a topological semimetal, *Nature Physics* **13**, 842 (2017).
 - [30] X. Yang, K. Burch, and Y. Ran, Divergent bulk photovoltaic effect in weyl semimetals, arXiv preprint arXiv:1712.09363 (2017).
 - [31] L. Wu, S. Patankar, T. Morimoto, N. L. Nair, E. Thewalt, A. Little, J. G. Analytis, J. E. Moore, and J. Orenstein, Giant anisotropic nonlinear optical response in transition metal mononpnictide weyl semimetals, *Nature Physics* **13**, 350 (2017).
 - [32] F. Flicker, F. de Juan, B. Bradlyn, T. Morimoto, M. G. Vergniory, and A. G. Grushin, Chiral optical response of multifold fermions, *Phys. Rev. B* **98**, 155145 (2018).
 - [33] L. E. Golub and E. L. Ivchenko, Circular and magnetoinduced photocurrents in weyl semimetals, *Phys. Rev.*

- B **98**, 075305 (2018).
- [34] T. Morimoto, M. Nakamura, M. Kawasaki, and N. Nagaosa, Current-voltage characteristic and shot noise of shift current photovoltaics, *Phys. Rev. Lett.* **121**, 267401 (2018).
 - [35] Y. Zhang, H. Ishizuka, J. van den Brink, C. Felser, B. Yan, and N. Nagaosa, Photogalvanic effect in weyl semimetals from first principles, *Phys. Rev. B* **97**, 241118 (2018).
 - [36] G. B. Osterhoudt, L. K. Diebel, M. J. Gray, X. Yang, J. Stanco, X. Huang, B. Shen, N. Ni, P. J. Moll, Y. Ran, *et al.*, Colossal mid-infrared bulk photovoltaic effect in a type-i weyl semimetal, *Nature materials* **18**, 471 (2019).
 - [37] J. Ma, Q. Gu, Y. Liu, J. Lai, P. Yu, X. Zhuo, Z. Liu, J.-H. Chen, J. Feng, and D. Sun, Nonlinear photoresponse of type-ii weyl semimetals, *Nature Materials* **18**, 476 (2019).
 - [38] D. Rees, K. Manna, B. Lu, T. Morimoto, H. Borrmann, C. Felser, J. E. Moore, D. H. Torchinsky, and J. Orenstein, Helicity-dependent photocurrents in the chiral weyl semimetal rhsi, *Science Advances* **6**, 10.1126/sciadv.aba0509 (2020).
 - [39] S. Kaushik and J. Cano, Magnetic photocurrents in multifold weyl fermions, arXiv preprint arXiv:2107.05106 (2021).
 - [40] X. Wan, A. M. Turner, A. Vishwanath, and S. Y. Savrasov, Topological semimetal and fermi-arc surface states in the electronic structure of pyrochlore iridates, *Phys. Rev. B* **83**, 205101 (2011).
 - [41] N. P. Armitage, E. J. Mele, and A. Vishwanath, Weyl and dirac semimetals in three-dimensional solids, *Rev. Mod. Phys.* **90**, 015001 (2018).
 - [42] Z.-M. Yu, Z. Zhang, G.-B. Liu, W. Wu, X.-P. Li, R.-W. Zhang, S. A. Yang, and Y. Yao, Encyclopedia of emergent particles in three-dimensional crystals, arXiv preprint arXiv:2102.01517 (2021).
 - [43] G. Chang, B. J. Wieder, F. Schindler, D. S. Sanchez, I. Belopolski, S.-M. Huang, B. Singh, D. Wu, T.-R. Chang, T. Neupert, S.-Y. Xu, H. Lin, and M. Z. Hasan, Topological quantum properties of chiral crystals, *Nature Materials* **17**, 978 (2018).
 - [44] G. Chang, J.-X. Yin, T. Neupert, D. S. Sanchez, I. Belopolski, S. S. Zhang, T. A. Cochran, Z. c. v. b. a. Chéng, M.-C. Hsu, S.-M. Huang, B. Lian, S.-Y. Xu, H. Lin, and M. Z. Hasan, Unconventional photocurrents from surface fermi arcs in topological chiral semimetals, *Phys. Rev. Lett.* **124**, 166404 (2020).
 - [45] P. Hosur, Circular photogalvanic effect on topological insulator surfaces: Berry-curvature-dependent response, *Phys. Rev. B* **83**, 035309 (2011).
 - [46] L. Braun, G. Mussler, A. Hruban, M. Konczykowski, T. Schumann, M. Wolf, M. Müntenberg, L. Perfetti, and T. Kampfrath, Ultrafast photocurrents at the surface of the three-dimensional topological insulator bi₂se₃, *Nature Communications* **7**, 13259 (2016).
 - [47] K. W. Kim, T. Morimoto, and N. Nagaosa, Shift charge and spin photocurrents in dirac surface states of topological insulator, *Phys. Rev. B* **95**, 035134 (2017).
 - [48] Q. Wang, J. Zheng, Y. He, J. Cao, X. Liu, M. Wang, J. Ma, J. Lai, H. Lu, S. Jia, D. Yan, Y. Shi, J. Duan, J. Han, W. Xiao, J.-H. Chen, K. Sun, Y. Yao, and D. Sun, Robust edge photocurrent response on layered type ii weyl semimetal wte₂, *Nature Communications* **10**, 5736 (2019).
 - [49] S. Chi, F. Liang, H. Chen, W. Tian, H. Zhang, H. Yu, G. Wang, Z. Lin, J. Hu, and H. Zhang, Surface nonlinear optics on centrosymmetric dirac nodal-line semimetal zrsi₂, *Advanced Materials* **32**, 1904498 (2020).
 - [50] H. Pan, X. Li, F. Zhang, and S. A. Yang, Perfect valley filter in a topological domain wall, *Phys. Rev. B* **92**, 041404 (2015).
 - [51] G. D. Mahan, *Many Particle Physics*, 3rd. ed. (New York, 2000).
 - [52] See Supplemental Materials for the details about the derivation of Eq. (5) in the main text, the symmetry analysis of nonzero shift conductivities of (001) surface, and the band structure of the Dirac lattice model.
 - [53] Y. Q. Huang, Y. X. Song, S. M. Wang, I. A. Buyanova, and W. M. Chen, Spin injection and helicity control of surface spin photocurrent in a three dimensional topological insulator, *Nature Communications* **8**, 15401 (2017).
 - [54] B. Q. Lv, T. Qian, and H. Ding, Experimental perspective on three-dimensional topological semimetals, *Rev. Mod. Phys.* **93**, 025002 (2021).
 - [55] G. Chang, S.-Y. Xu, B. J. Wieder, D. S. Sanchez, S.-M. Huang, I. Belopolski, T.-R. Chang, S. Zhang, A. Bansil, H. Lin, and M. Z. Hasan, Unconventional chiral fermions and large topological fermi arcs in rhsi, *Phys. Rev. Lett.* **119**, 206401 (2017).
 - [56] M. Neupane, S.-Y. Xu, R. Sankar, N. Alidoust, G. Bian, C. Liu, I. Belopolski, T.-R. Chang, H.-T. Jeng, H. Lin, A. Bansil, F. Chou, and M. Z. Hasan, Observation of a three-dimensional topological dirac semimetal phase in high-mobility cd₃as₂, *Nature Communications* **5**, 3786 (2014).
 - [57] S.-Y. Xu, C. Liu, S. K. Kushwaha, R. Sankar, J. W. Krizan, I. Belopolski, M. Neupane, G. Bian, N. Alidoust, T.-R. Chang, H.-T. Jeng, C.-Y. Huang, W.-F. Tsai, H. Lin, P. P. Shibayev, F.-C. Chou, R. J. Cava, and M. Z. Hasan, Observation of fermi arc surface states in a topological metal, *Science* **347**, 294 (2015).
 - [58] B. Q. Lv, S. Muff, T. Qian, Z. D. Song, S. M. Nie, N. Xu, P. Richard, C. E. Matt, N. C. Plumb, L. X. Zhao, G. F. Chen, Z. Fang, X. Dai, J. H. Dil, J. Mesot, M. Shi, H. M. Weng, and H. Ding, Observation of fermi-arc spin texture in taas, *Phys. Rev. Lett.* **115**, 217601 (2015).
 - [59] K. Deng, G. Wan, P. Deng, K. Zhang, S. Ding, E. Wang, M. Yan, H. Huang, H. Zhang, Z. Xu, J. Denlinger, A. Fedorov, H. Yang, W. Duan, H. Yao, Y. Wu, S. Fan, H. Zhang, X. Chen, and S. Zhou, Experimental observation of topological fermi arcs in type-ii weyl semimetal mote₂, *Nature Physics* **12**, 1105 (2016).
 - [60] D. Takane, Z. Wang, S. Souma, K. Nakayama, T. Nakamura, H. Oinuma, Y. Nakata, H. Iwasawa, C. Cacho, T. Kim, K. Horiba, H. Kumigashira, T. Takahashi, Y. Ando, and T. Sato, Observation of chiral fermions with a large topological charge and associated fermi-arc surface states in cosi, *Phys. Rev. Lett.* **122**, 076402 (2019).
 - [61] X.-P. Li, K. Deng, B. Fu, Y. Li, D.-S. Ma, J. Han, J. Zhou, S. Zhou, and Y. Yao, Type-iii weyl semimetals: (TaSe₄)₂I, *Phys. Rev. B* **103**, L081402 (2021).